AIAA-2005-0523

43rd AIAA Aerospace Sciences Meeting and Exhibit, January 10-13 2005, Reno NV

Analysis of Transition-Sensitized Turbulent Transport Equations

Christopher L. Rumsey*

NASA Langley Research Center, Hampton, VA 23681-2199, USA

William D. Thacker†

St. Louis University, St. Louis, MO 63156, USA

Thomas B. Gatski‡

NASA Langley Research Center, Hampton, VA 23681-2199, USA

Chester E. Grosch§

Old Dominion University, Norfolk, VA 23529, USA

The dynamics of an ensemble of linear disturbances in boundary-layer flows at various Reynolds numbers is studied through an analysis of the transport equations for the mean disturbance kinetic energy and energy dissipation rate. Effects of adverse and favorable pressure-gradients on the disturbance dynamics are also included in the analysis. Unlike the fully turbulent regime where nonlinear phase scrambling of the fluctuations affects the flow field even in proximity to the wall, the early stage transition regime fluctuations studied here are influenced across the boundary layer by the solid boundary. The dominating dynamics in the disturbance kinetic energy and dissipation rate equations are described. These results are then used to formulate transition-sensitized turbulent transport equations, which are solved in a two-step process and applied to zero-pressure-gradient flow over a flat plate. Computed results are in good agreement with experimental data.

I. Introduction

A current challenge in the prediction of wall-bounded turbulent flow fields within the realm of single-point closures is to consistently predict the (upstream) flow field and location of the natural transition region. The most widely used method for predicting natural transition is the e^N method (see, for example, Drela and Giles[1]), combined in some fashion to a turbulent flow solver. But this technique can be cumbersome and often requires considerable effort on the part of the user.[2]

Schmidt and Patankar[3] analyzed the natural capability of low-Reynolds-number K-ε models to simulate boundary-layer transition. Although there were significant limitations regarding accuracy, the models were considered to be useful as predictive engineering tools. Wilcox[4] took advantage of the capability of two-equation models to describe nonlinear growth of flow instabilities to develop a modified K-ω model that predicts transition. Walters and Leylek[5] developed a single-point method that accounted for the growth of Tollmien-Schlichting waves (for natural transition) and also employed an additional transport equation to represent the growth of nonturbulent streamwise fluctuations (for bypass transition). Wang and Perot[6] applied a non-equilibrium turbulent potential model to both natural and bypass transition.

*Senior Research Scientist, Computational Modeling and Simulation Branch, Mail Stop 128, Associate Fellow AIAA.

†Professor, Department of Physics, Parks College.

‡Senior Research Scientist, Computational Modeling and Simulation Branch, Mail Stop 128.

§Professor, Departments of Oceanography and Computer Science.

Examples of other transition-sensitized turbulence models, applicable to naturally transitioning flows, exist in the literature,[7–10] but their development has been based more on empirical grounds. In contrast, transition-sensitized turbulence models, applicable to intermittent flows[11] and flows with bypass transition,[12,13] have been extensively studied and refined over the last decade.

Motivated by the success of models in flows with bypass transition, a methodology is pursued here that can lead to the development of models applicable to generic flows in a natural, low-disturbance environment. In order to develop a general linkage between the transitioning laminar flow and the turbulent flow in a developing boundary layer, it is necessary to have a common mathematical framework from which the disturbances in both regimes can be described. In previous studies,[14,15] such a framework was developed by coupling a deterministic description of the evolution of disturbances in the laminar regime with an analysis of an ensemble of such disturbances. The approach was based on the observation that, even in the laminar regime, every flow is subject to an inevitable uncertainty in initial conditions. Therefore, although each individual disturbance evolves deterministically, a probability distribution must be introduced for the calculation of ensemble mean properties of the various disturbance statistical moments.

The mathematical methodology developed previously is now extended to a spatially developing boundary layer. This study focuses on the earliest stages of transition in a low disturbance environment where the disturbance amplitudes are small enough that nonlinear interactions can be neglected. Most current Reynolds-averaged Navier-Stokes (RANS) type closure models have difficulty representing pre-transition flow fields and transition location, particularly with nonzero pressure gradients or for three dimensional mean flows. Although three dimensional mean flows are not considered here, the effects of zero, favorable, and adverse pressure gradients on the kinetic energy and dissipation rate budgets are considered. The information obtained from these balance equations is used to guide the formulation of a unified model, which is then applied to the flow over a flat plate in zero pressure gradient.

II. Theory

A flat, solid-walled boundary is considered. The incompressible flow analysis focuses on downstream locations away from any leading-edge effects. The three-dimensional, laminar disturbance modes under consideration are bounded solutions of the linearized Navier-Stokes equations. Linear disturbance fields are generated that are deviations from an ensemble-mean boundary-layer velocity field given by the Falkner-Skan family of solutions, $U(Re, \beta, x_2)$, applicable to flow fields with zero, adverse and favorable pressure gradients. The effects of pressure gradient are introduced through the parameter β: $\beta = 0$, zero pressure gradient; $\beta < 0$, adverse pressure gradient; $\beta > 0$, favorable pressure gradient.

The velocity and pressure disturbance fields can be constructed from disturbance mode solutions by considering an ensemble of linear superpositions of modes with mode amplitudes $\Phi(\omega, k_3, x_{10})$ so that

$$u_i(\mathbf{x}, t) = \int d\omega\, dk_3 dx_{10}\, \Phi(\omega, k_3, x_{10}) \hat{u}_i(x_2, \omega, k_3, Re) e^{i\left(\int_{x_{10}}^{x_1} k_1 dx_1' + k_3 x_3 - \omega t\right)} \tag{1}$$

$$p(\mathbf{x}, t) = \int d\omega\, dk_3 dx_{10}\, \Phi(\omega, k_3, x_{10}) \hat{p}(x_2, \omega, k_3, Re) e^{i\left(\int_{x_{10}}^{x} k_1 dx_1' + k_3 x_3 - \omega t\right)} \tag{2}$$

where $(k_1(Re, \omega, k_3), 0, k_3)$ is the wave vector in coordinate directions (x_1, x_2, x_3) associated with the most unstable mode, (k_1 complex and k_3 real), ω is the (real) frequency, x_{10} is the position where the disturbance mode originates, and $\hat{u}_i$ and $\hat{p}$ are the disturbance velocity and pressure profiles for the most unstable mode. This ensemble is described by a probability distribution for the amplitudes so that their mean, $\langle \Phi(\omega, k_3, x_{10}) \rangle$ is zero, and covariance is homogeneous (x_1 and x_3-directions) and stationary,

$$\langle \Phi^*(\omega, k_3, x_{10}) \Phi(\omega', k_3', x_{10}') \rangle = \delta(\omega - \omega') \delta(k_3 - k_3') \delta(x_{10} - x_{10}') P(\omega, k_3, x_{10}). \tag{3}$$

Assuming that ω, k_3, and x_{10} are independent random variables, the probability density $P(\omega, k_3, x_{10})$ is partitioned as

$$P(\omega, k_3, x_{10}) = P_\omega(\omega) P_{k_3}(k_3) P_{x_{10}}(x_{10}). \tag{4}$$

The frequency space probability density $P_\omega(\omega)$ is assumed to correspond to band limited white noise with a flat spectrum

$$P_\omega(\omega) = \begin{cases} \dfrac{1}{\omega_H - \omega_L} & \omega_L < \omega < \omega_H \\ 0 & \text{otherwise} \end{cases} \tag{5}$$

where $\omega_L = 0.04$ and $\omega_H = 0.08$ are chosen to encompass the region of disturbance growth computed from linear stability theory. For the spanwise wavenumber probability density, the central limit theorem argues in favor of a Gaussian

$$P_{k_3}(k_3) = \frac{1}{\sqrt{2\pi\sigma^2}} \exp\left(-\frac{k_3^2}{2\sigma^2}\right) \tag{6}$$

with variance σ^2 large enough to encompass a sufficient range of energetic oblique modes. It was found that the results did not change for $\sigma \geq 0.1$. In this study $\sigma = 0.1$ was chosen and k_3 values ranged from -0.3 to 0.3. The disturbance modes are assumed to originate with equal probability along the boundary layer in accordance with the assumed homogeneity of the freestream turbulence field. In order to ensure that the same disturbance ensemble is generated at each streamwise location x_1, the probability density function $P_{x_{10}}(x_{10})$ is chosen to have the form

$$P_{x_{10}}(x_{10}) = \delta(x_1 - x_{10}) \tag{7}$$

This eliminates the exponential growth factor in Eqs. (1) and (2), and ensures that each disturbance mode has the same weight.

The second-moment correlations can be formed from the disturbance velocity and pressure fields given in Eqs. (1) and (2). For example, the disturbance stress tensor is given by

$$\begin{aligned} \tau_{ij}(x_1, x_2) &= \frac{1}{2}\left\langle u_i^* u_j + u_i u_j^* \right\rangle \\ &= \frac{1}{2}\int d\omega\, dk_3\, P_\omega(\omega) P_{k_3}(k_3) \left(\hat{u}_i^* \hat{u}_j + \hat{u}_i \hat{u}_j^*\right), \end{aligned} \tag{8}$$

with the disturbance kinetic energy, $K = \tau_{ii}/2$, and the disturbance isotropic dissipation rate is given by

$$\begin{aligned} \varepsilon(x_1, x_2) &= \frac{1}{Re}\left\langle \frac{\partial u_j}{\partial x_k} \frac{\partial u_j^*}{\partial x_k} \right\rangle \\ &= \frac{1}{Re}\int d\omega\, dk_3\, P_\omega(\omega) P_{k_3}(k_3) \\ &\quad \times \left[\left(|k_1|^2 + k_3^2\right)\hat{u}_j^* \hat{u}_j + \frac{d\hat{u}_j^*}{dx_2}\frac{d\hat{u}_j}{dx_2}\right] \end{aligned} \tag{9}$$

Note that, although streamwise homogeneity in the choice of ensemble has been maintained, all disturbance correlations retain a dependence on x_1 through either a direct Reynolds number dependence (as in the disturbance dissipation rate) or through the implicit Reynolds number dependence of $\hat{u}_i$ and k_1. Finally, in order to compare results at different values of Re_θ and β, the kinetic energy of the disturbance field at each Re_θ and β is normalized such that the integral of the kinetic energy across the boundary layer in x_2 is unity. It is now possible, from these quantities, to construct a detailed mapping of the ensemble-averaged disturbance field.

A. Disturbance energy budget

The derivation of the transport equations for the disturbance kinetic energy, $K = \tau_{ii}/2$, follows directly from the linearized Navier-Stokes equations coupled with an average over an ensemble of disturbances described by the distribution $P(\omega, k_3, x_{10})$. The resulting transport equation can be written as

$$\frac{DK}{Dt} = \mathcal{P} - \varepsilon + \Pi + \mathcal{D} \tag{10}$$

where

$$\mathcal{P} = -\tau_{12}\frac{dU}{dx_2} \tag{11}$$

$$\Pi = -\frac{1}{2}\frac{\partial}{\partial x_j}\left\langle u_j^* p + u_j p^* \right\rangle \tag{12}$$

$$\mathcal{D} = \frac{1}{Re}\frac{\partial^2 K}{\partial x_j \partial x_j} \tag{13}$$

are, respectively, the disturbance energy production, pressure-transport of disturbance energy, and viscous diffusion of disturbance energy. The disturbance energy dissipation rate is ε given in Eq. (9).

Using the solutions u_i and p (Eqs. (1) and (2)) obtained from the linearized disturbance equations coupled with the probability density distribution (Eq. (4)), the components of the disturbance energy equation can be obtained. It is instructive to examine the behavior of the disturbance ensemble at different streamwise locations. At low Re_θ (not shown) where there are no growing modes in the ensemble, the disturbance kinetic energy decays ($DK/Dt < 0$) because production, the contribution from dissipation and viscous diffusion are all negative. Only pressure-transport contributes positively to the energetic balance over most of the layer. Very near the wall, the dynamic balance is between the kinetic energy dissipation rate and viscous diffusion, which is analogous to the fully turbulent case very near the wall.

Figures 1 and 2 show the energy budget across the boundary layer at two different values of Re_θ. At each value of Re_θ, the distributions of energy production, dissipation rate, pressure-transport, and viscous diffusion are shown. Here DK/Dt is calculated as an instantaneous quantity, and not as a finite difference. Figure 1 shows the energy balance at $Re_\theta = 393$; a region of the flow where some modes included in the ensemble are unstable. At this value of Re_θ, there exists regions of the boundary layer where, for example, production is positive and pressure-transport is negative although overall $DK/Dt < 0$. Very near the wall the balance is predominantly between viscous diffusion and disturbance dissipation rate. Figure 2 shows the energy balance at $Re_\theta = 1040$. Increasing the Reynolds number causes an increase in the magnitudes of all of the terms in the balance. At larger values of Re_θ, the qualitative features of the energetic balance remain unchanged with only the tails of each distribution decaying more slowly with x_2^+ reflecting the downstream boundary-layer growth. At this and larger values of Re_θ, the kinetic energy is growing with $DK/Dt > 0$ across the boundary layer. Again, the near wall balance is between viscous diffusion and disturbance dissipation rate. It is apparent from Fig. 2 that, outside of the very near-wall region, the production and pressure-transport have opposite sign and are nearly proportional to one another although viscous diffusion also contributes to the balance. It is possible to show that this proportionality between the pressure-transport and energy production can be established through an analysis of the Poisson equation for the pressure fluctuations. In addition, the role of viscous diffusion in the dynamic balance across the boundary layer differs from the turbulent regime and changes with Reynolds number. In the fully turbulent case, the viscous diffusion changes sign with distance from the wall; however, for the linear disturbances examined here, the viscous diffusion is positive across the boundary layer at $Re = 1040$, and only changes sign at the lower Reynolds number.

The effect of imposed pressure gradient on the disturbance kinetic energy budget is shown in Figs. 3 and 4 at $Re_\theta \approx 1040$. In the adverse pressure gradient case ($\beta < 0$), the dynamic balance between the terms in the transport equation remain unchanged; however, there is a broadening of the distribution across the layer and an overall substantial increase in the amplitude levels associated with each term. For the favorable pressure gradient case shown in Fig. 4, the dynamic balance is significantly altered qualitatively from the zero pressure gradient case. The balance is more consistent with the $Re_\theta = 393$ zero pressure gradient case shown in Fig. 1. At this streamwise station, the ensemble of disturbances included both stable and unstable modes, but the overall balance showed a decay of disturbance kinetic energy across the boundary layer.

These results confirm that even though the individual disturbance modes satisfy the linear Navier-Stokes equations, an ensemble of such disturbances can display a complex range of energetic dynamics that characterize the early stage transition regime of a developing flow. In the next section, the dynamic balance of the disturbance dissipation rate is examined.

B. Disturbance dissipation rate budget

The transport equation for the disturbance dissipation rate ε is also directly derivable from the linearized momentum equations. The resulting form is given by

$$\frac{D\varepsilon}{Dt} = \underbrace{\mathcal{P}_\varepsilon^1 + \mathcal{P}_\varepsilon^2 + \mathcal{P}_\varepsilon^3}_{\mathcal{P}_\varepsilon} - \Upsilon + \Pi_\varepsilon + \mathcal{D}_\varepsilon \tag{14}$$

where

$$\mathcal{P}_\varepsilon^1 = -\frac{1}{Re}\frac{dU}{dx_2}\left\langle \frac{\partial u_1^*}{\partial x_j}\frac{\partial u_2}{\partial x_j} + \frac{\partial u_1}{\partial x_j}\frac{\partial u_2^*}{\partial x_j}\right\rangle \tag{15}$$

$$\mathcal{P}_\varepsilon^2 = -\frac{1}{Re}\frac{dU}{dx_2}\left\langle \frac{\partial u_j^*}{\partial x_1}\frac{\partial u_j}{\partial x_2} + \frac{\partial u_j}{\partial x_1}\frac{\partial u_j^*}{\partial x_2}\right\rangle \tag{16}$$

$$\mathcal{P}_\varepsilon^3 = -\frac{1}{Re}\frac{d^2U}{dx_2^2}\left\langle u_2^*\frac{\partial u_1}{\partial x_2} + u_2\frac{\partial u_1^*}{\partial x_2}\right\rangle \tag{17}$$

$$\Upsilon = \frac{2}{Re^2}\left\langle \frac{\partial^2 u_j^*}{\partial x_k \partial x_r}\frac{\partial^2 u_j}{\partial x_k \partial x_r}\right\rangle \tag{18}$$

$$\Pi_\varepsilon = -\frac{1}{Re}\frac{\partial}{\partial x_j}\left\langle \frac{\partial u_j^*}{\partial x_k}\frac{\partial p}{\partial x_k} + \frac{\partial u_j}{\partial x_k}\frac{\partial p^*}{\partial x_k}\right\rangle \tag{19}$$

$$\mathcal{D}_\varepsilon = \frac{1}{Re}\frac{\partial^2 \varepsilon}{\partial x_i \partial x_i} \tag{20}$$

are, respectively, mixed production, production by mean velocity gradient, gradient production, destruction, pressure-transport, and viscous diffusion. (The notation used here is consistent with the notation used by Rodi and Mansour.[16]) Analogous to the treatment of the DK/Dt term, $D\varepsilon/Dt$ is not a finite difference but is computed as an instantaneous quantity.

Figures 5 and 6 show the balance of terms across the boundary layer for the disturbance dissipation rate budget. With the exception of the destruction and viscous diffusion of dissipation, which essentially balance out across the entire boundary layer, all terms are negligible. This behavior suggests that in the absence of a production mechanism associated with vortex stretching, a nonlinear effect, direct dissipation of disturbance energy is confined to regions in close proximity to the wall. In contrast with the disturbance energy balances, the same (qualitative) dynamic balance is achieved for the two values of Re_θ shown and was also found for all values of Re_θ at which these calculations were carried out ($Re_\theta \leq 2000$) The only change that was found was the broadening of the distribution across the layer with increasing Re_θ. While energetic equilibrium ($DK/Dt = 0$) only occurred at a single value of Re_θ, Fig. 5 shows that $D\varepsilon/Dt$ is very small and ≈ 0 compared to the dominant terms, destruction and viscous diffusion of dissipation, throughout the entire range of Re_θ values studied. In fact, it was found that $D\varepsilon/Dt$ was always at least three orders of magnitude smaller than the dominant terms.

Although not shown, the dissipation rate dynamics are relatively insensitive to the imposition of pressure gradient on the flow. This once again shows that the disturbance dissipation rate is not a (significant) contributor to the disturbance dynamics in the early stage transition regime.

III. Model

The Reynolds averaged Navier-Stokes approach for predicting turbulent flow fields continues to be the primary engineering tool for calculating entire flow fields at high Reynolds numbers. However, closure models ranging from

algebraic to differential stress models usually cannot correctly predict the transition process. Nevertheless, in wall-bounded flows for example, the success of a turbulence model is often judged by its ability to predict the developing flow field. Such an assessment is often clouded by the fact that the region of transition is not well-determined by the turbulence model.

In the previous section, a set of transport equations for the disturbance kinetic energy and (isotropic) dissipation rate were analyzed. The disturbance variables were ensemble averages of deterministic disturbances obtained from the linear Navier-Stokes equations, and associated with a chosen probability density function, Eq. (4). While the probability distribution associated with the linear disturbances may be different than that for the turbulent fluctuations, the means associated with both ensembles are formed similarly. Thus, as was done in the last section, quantities such as the kinetic energy and dissipation rate and their respective transport equations can be analyzed analogous to those associated with the turbulence fluctuations.

As assumed throughout this analysis, the ensemble of disturbances examined are representative of the disturbance field in the early stages of a naturally transitioning wall-bounded flow.[17] The budgets discussed earlier can then be used, as in the development of RANS models for turbulent flow, to develop a RANS-type model for the early stage transition regime. The low Reynolds number ($Re_\theta = 393$) results, where the kinetic energy production is negative, are not of interest here, since they represent a regime in which disturbances decay instead of transitioning into turbulence. Rather, the results for $Re_\theta = 1040$ with zero and adverse pressure gradient are relevant and will be used.

The focus of this analysis is on linear eddy viscosity two-equation models. The eddy viscosity is ordinarily associated with turbulence, but in the current analysis it is also considered a disturbance viscosity that applies to linear disturbances in the early stages of transition. As in the turbulent case, the task then is to determine closure models for the destruction, pressure transport, and diffusion terms that appear in the disturbance kinetic energy and dissipation rate equations. At the outset, it is actually necessary to only consider models for the pressure-transport and diffusion terms. The destruction of disturbance kinetic energy is governed by the disturbance dissipation rate equation itself.

The base K-ε turbulence equations chosen for the purposes of the current investigation are written:

$$\frac{DK}{Dt} = \mathcal{P} - \varepsilon + \frac{1}{\rho}\frac{\partial}{\partial x_j}\left[\left(\mu + \frac{\mu_T}{\sigma_K}\right)\frac{\partial K}{\partial x_j}\right] \tag{21}$$

$$\frac{D\varepsilon}{Dt} = \frac{\varepsilon}{K}C_{\varepsilon 1}\mathcal{P} - C_{\varepsilon 2}\frac{\varepsilon^2}{K}f_2 + \frac{1}{\rho}\frac{\partial}{\partial x_j}\left[\left(\mu + \frac{\mu_T}{\sigma_\varepsilon}\right)\frac{\partial \varepsilon}{\partial x_j}\right] \tag{22}$$

where $\mathcal{P} = -\tau_{ij}\partial U_i/\partial x_j \approx 2\nu_T S_{ij}S_{ij}$ is the production term, and the resulting eddy viscosity is given by:

$$\mu_T = \rho\nu_T = C_\mu f_\mu \rho\frac{K^2}{\varepsilon} \tag{23}$$

The constants are: $C_{\varepsilon 1} = 1.44$, $C_{\varepsilon 2} = 1.83$, $\sigma_k = 1.0$, $\sigma_\varepsilon = \kappa^2/[\sqrt{C_\mu}(C_{\varepsilon 2} - C_{\varepsilon 1})]$, $C_\mu = 0.09$, and $\kappa = 0.41$. The function f_2 is given by:

$$f_2 = 1 - \exp\left(-\frac{Re_K}{12.5}\right) \tag{24}$$

where $Re_K = \rho\sqrt{K}d/\mu$, and d is the distance to the nearest wall. For simplicity, the function f_μ (which is typically used to insure proper asymptotic behavior of the turbulent variables as the wall is approached) is currently taken to be unity.

Inspection of Fig. 2 shows that the plots of disturbance energy production, diffusion and pressure-transport assume similar shapes from $x_2^+ \approx 10$ to $x_2^+ \approx 60$, and combine to produce a positive DK/Dt. This suggests that the sum of these three terms may be modeled as an effective disturbance energy production $\mathcal{P}_d$. Regarding the dissipation rate equation, on the other hand, the data indicate that $D\varepsilon/Dt \approx 0$ throughout the layer. These ideas lead to the following possible forms for the modeled transport equations for the disturbance energy and dissipation rate:

$$\frac{DK}{Dt} = \mathcal{P}_d - \varepsilon \tag{25}$$

$$\frac{D\varepsilon}{Dt} = 0, \tag{26}$$

where $\mathcal{P}_d$ represents the sum $\mathcal{P} + \Pi + \mathcal{D}$ appearing in Eq. (10) and is modeled as $C_d\mathcal{P}'$. For this two equation formulation, a Boussinesq type relation is assumed for the disturbance shear stress so that the production $\mathcal{P}'$ can be written in the form $2\nu_d S_{ij}S_{ij}$, with ν_d the disturbance mode viscosity ($\nu_d = C_{\mu d}K^2/\varepsilon$).

In order to bridge together the two flow regimes (represented by Eqs. (21) & (22) and Eqs. (25) & (26)), an indicator function $\mathcal{I}$ is used. $\mathcal{I}$ represents the probability that the flow at any given point is turbulent, with $0 \leq \mathcal{I} \leq 1$. Thus, $\mathcal{I} = 0$ represents purely laminar flow and $\mathcal{I} = 1$ represents purely turbulent flow. The precise form that the $\mathcal{I}$-equation needs to take is an ongoing subject of active research. Currently, a provisional measure has been taken in an effort to reproduce the known dependence of transition on freestream turbulence intensity. This form of the $\mathcal{I}$-equation is derived below.

The original K and ε equations are modified using the function $\mathcal{I}$ such that when $\mathcal{I} = 1$ the fully turbulent equations are recovered, and when $\mathcal{I} = 0$ the laminar disturbance equations are recovered. (However, as an aid to improved numerical behavior of the solution, the disturbance form of the equations are modified to retain dissipation terms. The destruction term in the dissipation rate equation is also retained in order to prevent too-rapid freestream eddy viscosity decay.) The final forms of the K and ε equations are:

$$\frac{DK}{Dt} = (1-\mathcal{I})\mathcal{P}_d + \mathcal{I}\mathcal{P} - \varepsilon + \frac{1}{\rho}\frac{\partial}{\partial x_j}\left[\left(\mu + \mathcal{I}\frac{\mu_T}{\sigma_K}\right)\frac{\partial K}{\partial x_j}\right] \tag{27}$$

$$\frac{D\varepsilon}{Dt} = \mathcal{I}\frac{\varepsilon}{K}C_{\varepsilon 1}\mathcal{P} - C_{\varepsilon 2}\frac{\varepsilon^2}{K}f_2 + \frac{1}{\rho}\frac{\partial}{\partial x_j}\left[\left(\mu + \mathcal{I}\frac{\mu_T}{\sigma_\varepsilon}\right)\frac{\partial \varepsilon}{\partial x_j}\right] \tag{28}$$

Here, $\mathcal{P}_d \approx 2\nu_T S_{ij}S_{ij}(C_dC_{\mu d}/C_\mu)$, $C_d = 0.3$, and $C_{\mu d} = 0.026$.

The indicator function $\mathcal{I}$ should obey an evolution equation that produces the correct dependence of transition location on the freestream turbulence level Tu. As freestream turbulence increases the transition location for a flat plate boundary layer is known[18] to move forward along the boundary layer, i.e., to smaller values of streamwise coordinate. The indicator function should also be related to some local quantity that gives a measure of the level of turbulence within the boundary layer. Motivated by these considerations, the behavior of the turbulence Reynolds number $Re_t = \rho K^2/\mu\varepsilon$ was studied for laminar ($\mathcal{I} = 0$) solutions of Eqs. (27) and (28). (Note that Re_t is proportional to the eddy viscosity μ_T appearing in the production and transport terms of the disturbance kinetic energy and dissipation rate equations.) Figure 7 shows contour plots of Re_t for three different levels of Tu. The higher the freestream Tu, the higher the maximum Re_t levels, and the further forward the location where Re_t first exceeds the freestream level. This suggests that the rate of increase in the indicator function could be related to Re_t. As a first provisional attempt at constructing the $\mathcal{I}$-equation, a source term proportional to the local value of Re_t minus its freestream value was introduced. With this choice of source term, $\mathcal{I}$ begins to increase when Re_t exceeds its freestream value. A diffusion term was also included. This equation produced the desired dependency of transition location to freestream Tu, but it should be considered work-in-progress. (For example, a destruction term may also be desirable to provide relaminarization capability.) The current form of the indicator function transport equation is given by:

$$\frac{D\mathcal{I}}{Dt} = C_{\mathcal{I}}\mathcal{P}^*_{\mathcal{I}} + \frac{1}{\rho}\frac{\partial}{\partial x_j}\left[\frac{\mu_t}{\sigma_{\mathcal{I}}}\frac{\partial \mathcal{I}}{\partial x_j}\right] \tag{29}$$

where $\mathcal{P}_{\mathcal{I}} = Re_t - Re_{t,\infty}$, $C_{\mathcal{I}} = 4$ and $\sigma_{\mathcal{I}} = 1$. The production term is limited via $\mathcal{P}^*_{\mathcal{I}} = \min[\max(\mathcal{P}_{\mathcal{I}}, 0), 50]$, and $\mathcal{I}$ is limited to be between 0 and 1. Eqs. 27, 28, and 29 are solved in conjunction with the RANS equations. A specific procedure is necessary for obtaining consistent solutions to the equations:

1. First, solve only RANS plus the two disturbance equations (Eqs. 27 and 28 with $\mathcal{I}$ set to zero). This step establishes the "disturbance levels" of K and ε in the vicinity of the body. It is important that this step be fully converged (the final answer is strongly dependent on the level of convergence of this step).

2. Restart from the solution of the previous step using RANS plus all three equations, Eqs. 27, and 28, and 29.

The boundary conditions at solid walls are: $K_w = 0$, $(\partial\varepsilon/\partial n)_w = 0$, and $\mathcal{I}_w = 0$. At freestream inflow the three quantities are taken to be their freestream values, and at freestream outflow they are extrapolated from the interior of the domain.

The freestream conditions are established as follows. For the indicator function, $\mathcal{I}_\infty = 0$. Given a freestream turbulence intensity Tu (in percent, defined as $Tu \equiv 100\sqrt{2K/(3U_\infty^2)}$), the freestream nondimensional K_∞ is given by: $K'_\infty = K_\infty/a_\infty^2 = 1.5[(Tu)(M_\infty)/100]^2$. In the current methodology, the freestream $Re_{t,\infty}$ is taken to be proportional to K_∞. Therefore, freestream ε_∞ is proportional to K_∞. One advantage to using this relationship is that the resulting decay rate of the turbulence quantities in the freestream is identical regardless of freestream Tu. Currently: $\varepsilon'_\infty = \varepsilon_\infty\mu_\infty/(\rho_\infty a_\infty^4) = (5.4\times10^{-8})K'_\infty$. Table 1 gives freestream levels for various Tu, for $M_\infty = 0.2$.

Table 1. Example freestream levels for $M_\infty = 0.2$

Tu, percent	$K'_\infty = K_\infty/a_\infty^2$	$\varepsilon'_\infty = \varepsilon_\infty\mu_\infty/(\rho_\infty a_\infty^4)$	$Re_{t,\infty}$	$\mu_{t,\infty}$
0.042	1.058×10^{-8}	5.715×10^{-16}	0.20	0.018
0.1	6.000×10^{-8}	3.240×10^{-15}	1.11	0.10
0.2	2.400×10^{-7}	1.296×10^{-14}	4.44	0.40
0.26	4.056×10^{-7}	2.190×10^{-14}	7.51	0.68
0.34	6.936×10^{-7}	3.745×10^{-14}	12.8	1.15
0.70	2.940×10^{-6}	1.588×10^{-13}	54.4	4.90
1.25	9.375×10^{-6}	5.063×10^{-13}	173.6	15.6

Like the original k-ε model itself, the current method does not maintain freestream turbulence levels (i.e., there is decay of the turbulence quantities with distance from the inflow boundary, where freestream levels have been set). The current model also shares the characteristic that for high freestream Tu (greater than 0.5% or so), the freestream $Re_{t,\infty}$ (or $\mu_{t,\infty}$) levels can get very large. See Table 1. With unrealistically high background eddy viscosity levels, laminar regions in the flow are corrupted. Unfortunately, if one tries to correct this behavior by increasing ε_∞, then freestream decay rate becomes much too rapid. The current levels were chosen as a compromise between rapidity of decay (current freestream eddy viscosity decays to 74% of its inflow value by the time it reaches the plate leading edge) and having excessively high freestream eddy viscosity levels. In any case, the primary focus of this method is on natural transition, which should be applicable only for low Freestream Tu. A focus of future work will be developing the capability to maintain freestream turbulence levels in the method with little or no decay.

IV. Results

The method described in the last section was implemented into the finite-volume RANS code CFL3D of Krist et al.[19] Results were generated for a flat plate in zero pressure gradient, at Re = 6 million based on plate length and $M = 0.2$. All results were two-dimensional, described from this point forward by the (x, y) coordinate system notation. A fine grid of size (385×129) was used, along with a medium (193×65) and coarse (97×33) level created by using every other grid point from the next finer grid. The grid extended from an x-location of $-1/3$ to 1, with the plate itself located between 0 and 1. The grid extent in the y-direction was approximately 1. The minimum spacing at the wall yielded an average minimum $y+$ of approximately 0.2 on the fine grid, 0.5 on the medium grid, and 1.1 on the coarse grid.

Figure 8 shows skin friction coefficient results plotted as a function of Re_x ($= u_\infty x/\nu_\infty$) using the medium grid for a range of different Tu, from 0.042% to 1.25%. Transition start locations were taken from the experimental results of Schubauer and Skramstad[20] (for $0.042 < Tu < 0.344$), and from Abu-Ghannam and Shaw[18] (for $Tu = 1.25\%$). Computed results agreed well with the experiments at the intermediate levels ($0.1 < Tu < 0.34$). Although the results at $Tu = 1.25\%$ predicted the transition start location reasonably well, the computed C_f levels in general were

poor because of the corrupting influence of the too-high freestream eddy viscosity, as discussed in the last section. At $Tu = 0.042\%$, the computations predicted transition to be further aft than in the experiment. However, experiments often show widely different transition locations at very low Tu levels, due to different noise levels in the wind tunnels. See Wells.[21]

Sensitivity of the results to grid size are shown in Fig. 9, for the case with $Tu = 0.2\%$. The transition location changed by about 3.5% of the plate length between the medium and fine grids, and by about 5% between the coarse and medium grids. These levels of grid dependence are not surprising if one considers that the disturbance equations are likely to be quite sensitive to the streamwise gradients. The Re_x at the starting location of transition are plotted as a function of Tu in Fig. 10; the figure includes the effect of grid density. The experimental "best-fit" transition start location curve from Abu-Ghannam and Shaw[18] is also plotted. There was an excellent correspondence between the CFD results and the experimental correlation.

V. Conclusions

The dynamics of an ensemble of disturbances in boundary-layer flow with and without pressure gradient was studied. The individual disturbance modes were solutions of the linearized Navier-Stokes equations and the probability density function associated with the ensemble accounted for distributions in spanwise wavenumber, frequency and initial spatial position. Such an ensemble represents the early stages of a transition disturbance field which ultimately leads to a fully turbulent field.

An analysis of the dynamic balance in the disturbance kinetic energy and dissipation rate equations showed behavior that contrasted with the fully turbulent case at both low Reynolds numbers and in near-wall regions. This new insight was critical in properly representing the dynamics in the linear disturbance region. While no self-similar behavior was reached, the qualitative features of the dynamic balance became independent of Re_θ and showed that energy production, pressure-transport, and viscous diffusion dominated across the boundary layer with a small contribution from dissipation rate. The dissipation rate only played a role in very close proximity to the solid boundary where it balanced the energy diffusion.

The results obtained here provided new insight into the dynamic balance of an ensemble of disturbances in the early stages of a (naturally) transitioning boundary-layer flow in a low disturbance environment. The information was used to develop transport equations for the ensemble of disturbances, which were subsequently coupled using an intermittency function to corresponding transport equations valid in the fully turbulent regime. The resulting three-equation model was solved via a two-step procedure. Results for a zero-pressure-gradient flat plate agreed well with experimental data for freestream turbulence intensity levels at and below 0.34%. Transition locations were also predicted in good agreement with experiment at higher freestream intensities, but issues related to freestream turbulence decay corrupted the quality of those results. Developed from first principles, this method holds promise as a transition-prediction tool for the Reynolds-averaged Navier-Stokes equations, with no need for empirical correlations.

References

[1]M. Drela and M. B. Giles, "Viscous-Inviscid Analysis of Transonic and Low Reynolds Number Airfoils," AIAA J. **25**, No. 10, 1347–1355 (1987).

[2]H. W. Stock and W. Haase, "Feasibility Study of e^N Transition Prediction in Navier-Stokes Methods for Airfoils," AIAA J. **37**, No. 10, 1187–1196 (1999).

[3]R. C. Schmidt and S. V. Patankar, "Simulating Boundary Layer Transition with Low-Reynolds-Number k-ε Turbulence Models: Part 1 – An Evaluation of Prediction Characteristics," ASME J. Turbomachinery **113**, 10–17 (1991).

[4]D. C. Wilcox, "Simulation of Transition with a Two-Equation Turbulence Model," AIAA J. **32**, No. 2, 247–255 (1994).

[5]D. K. Walters and J. H. Leylek, "A New Model for Boundary Layer Transition Using a Single-Point RANS Approach," ASME J. Turbomachinery **126**, 193–202 (2004).

[6]C. Wang and B. Perot, "Prediction of Turbulent Transition in Boundary Layers Using the Turbulent Potential Model," J. Turbulence **3**, 22–36 (2004).

[7]Y. B. Suzen and P. G. Huang, "Modeling of Flow Transition Using an Intermittency Transport Equation," ASME J. Fluid Eng. **122**, 273–284 (2000).

[8]E. S. Warren and H. A. Hassan, "Transition Closure Model for Predicting Transition Onset," J. Aircraft **35**, No. 5, 769–775 (1998).

[9]F. R. Menter, R. B. Langtry, S. R. Likki, Y. B. Suzen, P. G. Huang, S. Volker, "A Correlation-Based Transition Model Using Local Variables, Part 1 - Model Formulation," Paper GT2004-53452, Proceedings of ASME Turbo Expo 2004, June 14-17, Vienna, Austria (2004).

[10]D. Marinov and Z. Zapryanov, "Numerical Modelling of Laminar-Turbulent Transition in the Boundary Layers Under the Influence of Low Free-Stream Turbulence Intensities," Comput. Meth. in Applied Mech. & Eng. **110**, 263–273 (1993).

[11]J. R. Cho and M. K. Chung, "A k-ε-γ Equation Turbulence Model," J. Fluid Mech. **237**, 301–322 (1992).

[12]J. Steelant and E. Dick, "Modeling of Bypass Transition with Conditioned Navier-Stokes Equations Coupled to an Intermittency Transport Equation," Int. J. Num. Meth. Fluids **23**, 193–220 (1996).

[13]A. M. Savill, "By-pass Transition Using Conventional Closures," In: Closure Strategies for Modelling Turbulent and Transitional Flows (B. E. Launder and N. D. Sandham, eds.), Cambridge University Press, Cambridge, 464–492 (2001).

[14]W. D. Thacker, T. B. Gatski and C. E. Grosch, "Analyzing Mean Transport Equations of Turbulence and Linear Disturbances in Decaying Flows," Phys. Fluids **11**, No. 9, 2626–2631 (1999).

[15]W. D. Thacker, C. E. Grosch and T. B. Gatski, "Modeling the Dynamics of Ensemble-Averaged Linear Disturbances in Homogeneous Shear Flow," Flow Turbul. Combust. **63**, 39–58 (1999).

[16]W. Rodi and N. N. Mansour, "Low Reynolds Number $k-\varepsilon$ Modelling with the Aid of Direct Simulation Data," J. Fluid Mech. **250**, 509–529 (1993).

[17]J. Cohen, K. S. Breuer, and J. H. Haritonidis, "On the Evolution of a Wave Packet in a Laminar Boundary Layer," J. Fluid Mech. **225**, 575–606 (1991).

[18]B. J. Abu-Ghannam and R. Shaw, "Natural Transition of Boundary Layers - The Effects of Turbulence, Pressure Gradient, and Flow History," J. Mech. Eng. Sci. **22**, No. 5, 213–228 (1980).

[19]S. L. Krist, R. T. Biedron, and C. L. Rumsey, "CFL3D User's Manual (Version 5.0)", NASA TM-1998-208444, June 1998.

[20]G. B. Schubauer and H. K. Skramstad, "Laminar Boundary Layer Oscillations and Transition on a Flat Plate," NACA Rept. 909, 1948.

[21]C. S. Wells, Jr., "Effects of Freestream Turbulence on Boundary-Layer Transition," AIAA J. **5**, No. 1, 172–174 (1967).

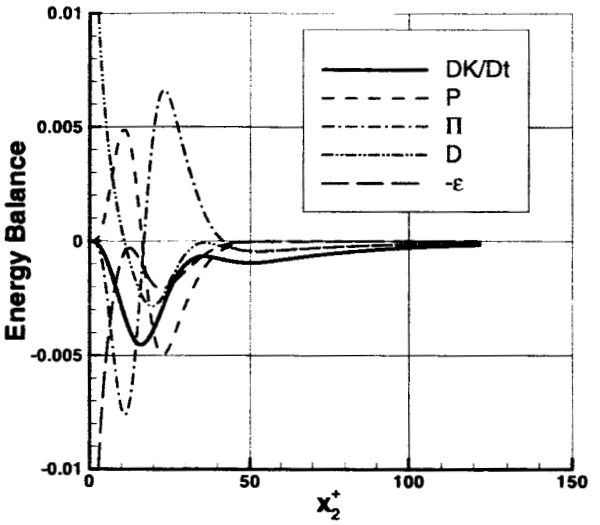

Figure 1. Disturbance energy balance at different downstream positions (zero pressure gradient), $Re_\theta = 393$.

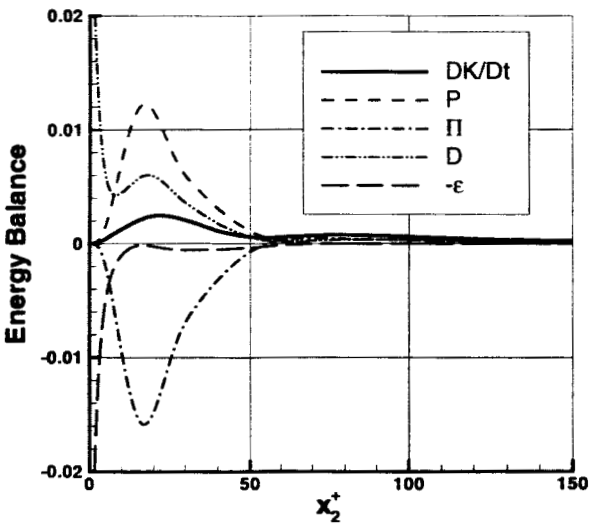

Figure 2. Disturbance energy balance at different downstream positions (zero pressure gradient), $Re_\theta = 1040$.

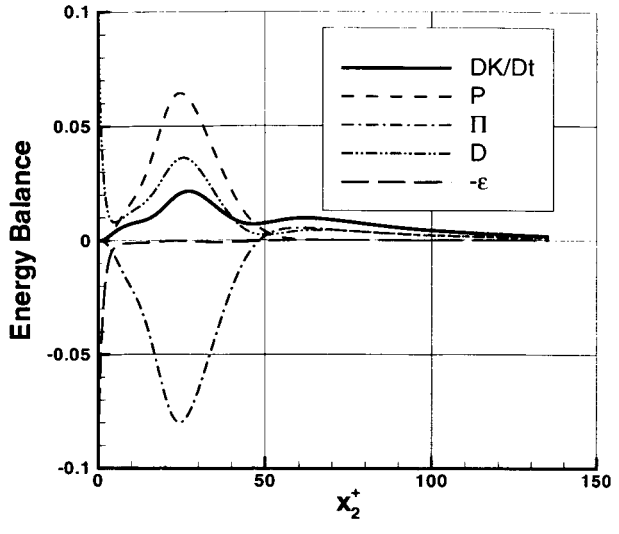

Figure 3. Effect of adverse pressure gradient ($\beta = -0.15$) on disturbance kinetic energy balance, $Re_\theta = 1045$.

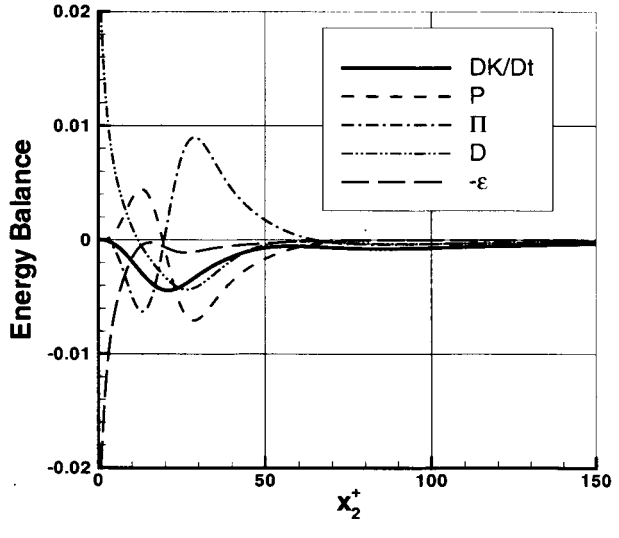

Figure 4. Effect of favorable pressure gradient ($\beta = 0.15$) on disturbance kinetic energy balance, $Re_\theta = 1041$.

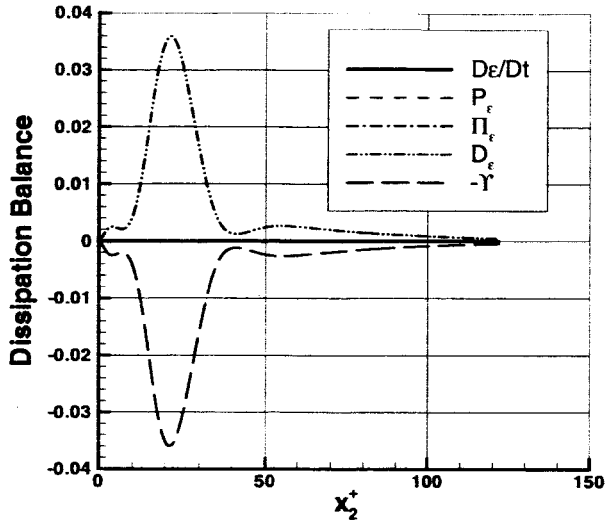

Figure 5. Disturbance dissipation rate balance at different downstream positions (zero pressure gradient), $Re_\theta = 393$.

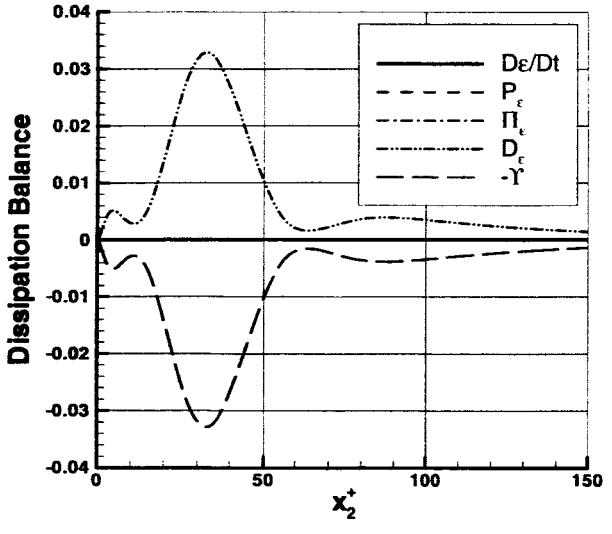

Figure 6. Disturbance dissipation rate balance at different downstream positions (zero pressure gradient), $Re_\theta = 1040$.

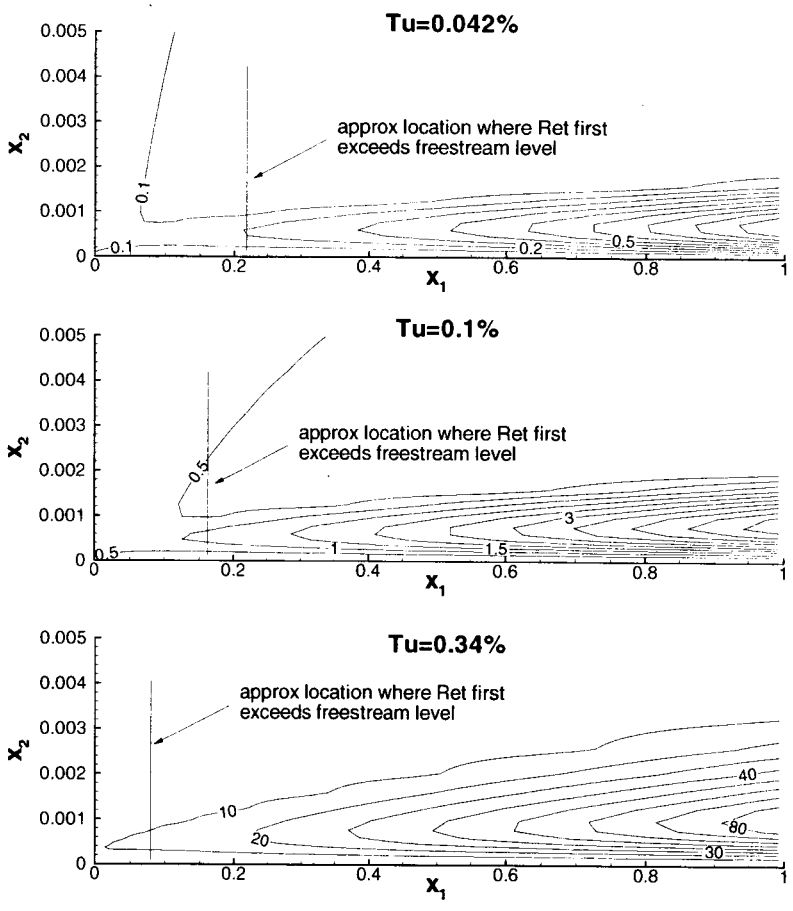

Figure 7. Contour plots of Re_t over flat plate ($M = 0.2$, $Re = 6 \times 10^6$) for three different freestream Tu levels, using disturbance equations.

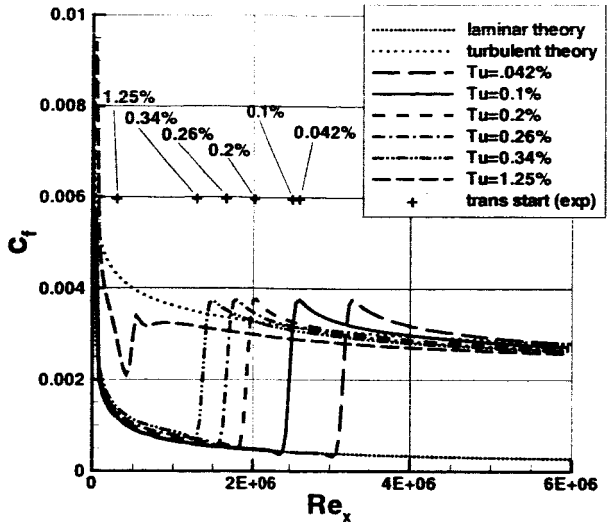

Figure 8. Skin friction coefficients on flat plate for different Tu, medium grid.

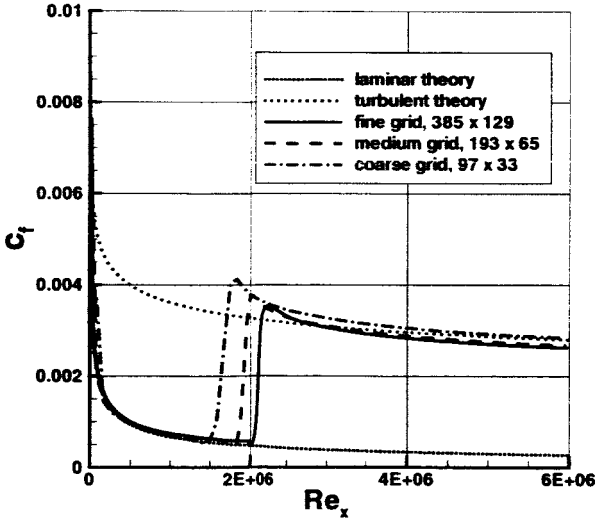

Figure 9. Grid density effect on skin friction coefficient for flat plate, $Tu = 0.2\%$.

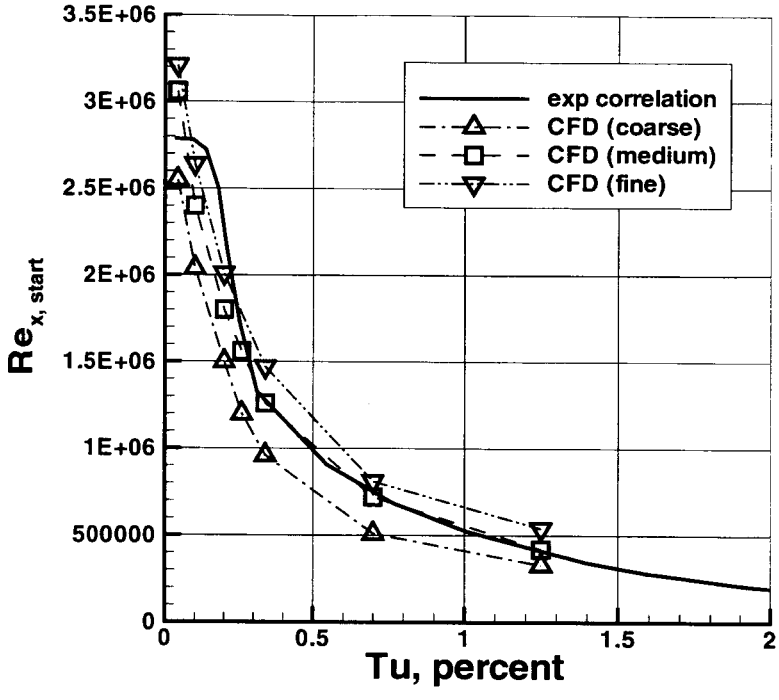

Figure 10. Re_x **at transition start location for flat plate as a function of** Tu**.**